Available online at www.sciencedirect.com
ScienceDirect
Journal of Magnetic Resonance 182 (2006) 143–151
JMR Journal of Magnetic Resonance
www.elsevier.com/locate/jmr

Multiecho sequence for velocity imaging in inhomogeneous rf fields

S. Ahola [a,b], J. Perlo [a], F. Casanova [a], S. Stapf [a], B. Blümich [a,*]

[a] Institut für Technische Chemie und Makromolekulare Chemie, RWTH Aachen, D-52056, Germany
[b] University of Oulu, Department of Physical Sciences, Finland

Received 24 April 2006; revised 14 June 2006
Available online 13 July 2006

Abstract

The unambiguous determination of velocities with spatial resolution in a multiecho PFG NMR sequence strongly depends on the homogeneity of the B_1 field. This affects, in particular, the use of surface coils that bear considerable potential for on-line flow monitoring where a fast-imaging sequence can become vital. However, even with most rf coils dedicated for imaging applications, B_1 inhomogeneities are sufficiently large to generate severe problems in performing velocity-imaging experiments. In this paper, the use of a combination of different phase cycles in Carr–Purcell sequences is discussed. The suggested phase cycling scheme tolerates large flip angle imperfections arising in inhomogeneous B_1 fields, and thus allows acquisition of a maximum number of echoes within a pulse train. The performance of the velocity-imaging sequence is proven by using phantom samples developing known laminar flow patterns.
© 2006 Elsevier Inc. All rights reserved.

Keywords: NMR microscopy; Flow; Multiecho; RARE; FSE; TSE; Surface coil; Velocity measurements

1. Introduction

NMR imaging has the extraordinary advantage of resolving not only spin density, but a wealth of other parameters like relaxation times, chemical shift, and even molecular displacement. Often these parameters can be encoded easily by combining suitable delay times or multipulse modules with one of the different fast-imaging acquisition schemes. However, one particular problem might arise if motion, especially coherent flow, has to be detected with spatial resolution. First of all, the total displacement of spins needs to be restricted to the pixel or voxel size; otherwise erroneous assignments of velocities will occur. Second, a frequently used approach to encode velocities is via phase encoding which requires the phase of the signal to be preserved correctly throughout the pulse sequence up to the acquisition period.

Magnitude information can be used, for instance, in time-of-flight experiments where a subset of spins is marked by appropriately shaped pulse excitations and the evolution of this pattern is visualized [1,2]. These techniques, however, are aimed at particular problems where displacements need to exceed the pixel size, and they are often compromised by blurring effects so that their primary goal is to visualize flow patterns rather than to quantify the velocity field, although, in principle, velocity profiles can be reconstructed [3].

Another approach is the acquisition of a succession of fast images from which information of motion is deduced. This method can be applied to processes that are instationary on timescales exceeding the image acquisition time, and their temporal resolution depends on the repetition time. As is the case for tagging techniques, this procedure provides information about motion exceeding the pixel dimensions. A number of work has been reported which deduce transport parameters from a quick succession of spin-density images without velocity encoding [4,5]. In [6], the outflow effect has been used to reconstruct a velocity profile from a series of two-dimensional images.

In the literature, a growing number of applications have been presented that combine phase encoding of the velocity

* Corresponding author. Fax: +49 241 80 22185.
E-mail address: bluemich@mc.rwth-aachen.de (B. Blümich).

1090-7807/$ - see front matter © 2006 Elsevier Inc. All rights reserved.
doi:10.1016/j.jmr.2006.06.017

with fast imaging and thus directly generate a *velocity map*. This involves variations of the three principle classes of rapid imaging, i.e. successive use of fresh portions of the initial magnetization or steady-state conditions such as in FLASH [7], repeated use of the full magnetization by gradient echoes such as in EPI [8] or by spin echoes such as in RARE [9]. A fast repetition of pulses with interspersed velocity encoding gradients has been used for gases with short relaxation times [10], whereas low flip angle (FLASH-type) approaches have been reported for hyperpolarized gas flow [11] or slow flow in plants [12]. For substances with long relaxation times, the disadvantage of the technique lies in its reduced signal-to-noise ratio. A train of gradient echoes avoids the accumulation of rf pulse errors, but remains restricted to samples with long T_2^*.

Kose has pioneered the work on EPI applications to velocity mapping in fluid flow [13–15]. More recently, Sederman et al. used the repeated application of an EPI train to generate 3D velocity images in pipe flow [16]. Han and Callaghan [17] applied an EPI variant with interspersed π pulses [18] to transient motion in a biaxial extension cell. In this method, samples of shorter T_2^* but moderate T_2 become accessible but the sensitivity to pulse imperfections is reintroduced and has been taken care of by the use of composite rf pulses. Velocity encoding combined with RARE-imaging modules has successfully been applied by Scheenen et al. [19] to transport in plants and Manz [20] to pipe flow, where in both cases comparatively large and homogeneous rf coils were employed so that pulse imperfections did not become apparent.

The essential problem in phase-encoded velocimetry [21] is the need to preserve the signal phase during repeated application of rf and/or gradient pulses which are necessary requirements for fast-imaging sequences (see following section for a more detailed discussion). In ideal situations, such as in relatively homogeneous B_0 and B_1 fields, this can easily be achieved by assuming ''perfect'' rf pulses, i.e. pulses which define a uniform flip angle throughout the region of interest. B_1 inhomogeneities lead to position-dependent flip angles that are often acceptable in a conventional single-encoding experiment, but might accumulate to non-negligible errors upon application of pulse trains, and the initial signal phase—the relative weight of the sine and cosine components of the transverse magnetization carrying the encoding of velocity—is lost during the sequence. A scheme to preserve both components has, for instance, been described for a non-imaging technique in [22].

The latter effect is certainly observed for surface coils with their depth-dependent rf field. However, surface coils increase the flexibility of NMR imaging considerably since they can be purpose-built or optimized to samples of almost arbitrary shapes; organ and extremities coils in medical imaging and applications to flat, quasi-two-dimensional objects are among the fields where surface coils have turned out to be advantageous [23].

In this contribution, we demonstrate a method based on adequate phase cycling, calling it CP/CPMG-RARE, which provides a robust approach to fast-flow imaging, i.e. the combination of multiecho spin density imaging with phase-encoded velocimetry, in inhomogeneous B_1 fields. We have used a homebuilt surface-coil, but also a conventional birdcage coil in order to demonstrate that the method can be similarly beneficial for commercial coils with a limited B_1 field homogeneity.

In our approach, the robustness of multiecho acquisition with individual phase cycles is tested based on a RARE-type pulse sequence with the aim of acquiring the full 2D image information within a single echo train (i.e. without the need for k-space segmentation). We first discuss the performance of well-known phase cycles for the use of π pulse trains, and state the need to preserve both the sine and the cosine part of the echo, followed by a description of the influence of imperfect pulses on the propagator shape. The feasibility of the method is shown for laminar flow measured with a birdcage coil and a simple surface coil and compared to uncompensated multiecho experiments.

2. Theory: velocity measurements by PFG NMR

2.1. Phase encoding of velocity

During a standard PGSE sequence where the amplitude of the bipolar gradients is $\mathbf{G}$, their separation Δ and the pulse duration δ, a spin isochromat with velocity $\mathbf{v}$ will acquire a phase shift

$$\phi = \gamma\delta\Delta\mathbf{G}\mathbf{v} = 2\pi\mathbf{q}\Delta\mathbf{v} \tag{1}$$

with $\mathbf{q} = (2\pi)^{-1}\gamma\delta\mathbf{G}$. Thus, the velocity encoding generates a dephasing of the magnetization relative to its initial orientation immediately before the PFG encoding. Simultaneously, dephasing takes place due to background field gradients and chemical shift differences, but this contribution is usually refocused by the generation of a spin echo. Therefore, the echo phase is sensitive only to displacement.

In general, spins within a given volume element can possess a distribution of velocities. This so-called average propagator [24] can be measured by PFG NMR methods. More precisely, the average propagator represents the distribution of displacements during a time interval Δ. The NMR signal in the reciprocal space of displacement, i.e. $\mathbf{q}$-space, is weighted by the spin density and by a conditional probability $P(\mathbf{r}|\mathbf{r}', \Delta)$, which is the probability that a spin moves from $\mathbf{r}$ to $\mathbf{r}'$ during the interval Δ:

$$S(\mathbf{q}) = \int\int \rho(\mathbf{r})P(\mathbf{r}|\mathbf{r}', \Delta)\mathrm{e}^{-\mathrm{i}2\pi\mathbf{q}\cdot(r'-r)}\mathrm{d}\mathbf{r}\mathrm{d}\mathbf{r}' \tag{2}$$

Because the signal depends only on the net displacement $\mathbf{R} = \mathbf{r}' - \mathbf{r}$ and not on the starting point $\mathbf{r}$, the propagator can be written as

$$S(\mathbf{q}) = \int P(\mathbf{R}, \Delta)\mathrm{e}^{-\mathrm{i}2\pi\mathbf{q}\cdot\mathbf{R}}\mathrm{d}\mathbf{R} \tag{3}$$

Note that $P(\mathbf{R}, \Delta)$, is a real function, which will be exploited for the design of the pulse sequence below.

2.2. Multiecho sequences

Multiecho sequences offer several advantages compared to single-echo methods. In the context of PFG NMR, they can be exploited in either of the following ways: first, to add up all echoes and thus improve the signal-to-noise ratio; second, to determine the velocity distribution independently for each echo and obtain a correlation between displacement and relaxation time T_2; third, introduce additional encoding between the echoes such as imaging gradients in order to reconstruct a velocity-encoded image (note that the T_2 decay is still implicitly contained in the signal of this sequence).

We will discuss first a sequence where a single velocity-encoding step is preceding a CPMG detection module. The effect of the velocity encoding to the CPMG sequence is analogous to applying the excitation pulse with a particular phase ϕ. For the case $\phi = 0°$, the magnetization after the excitation pulse is parallel, in the rotating frame, to the refocusing pulses (phase 90°), thus the magnetization is preserved from echo to echo and a train of echoes decaying with a characteristic time constant T_2 is observed (Fig. 1a). In contrast, for $\phi = 90°$, the magnetization amplitude oscillates from echo to echo and vanishes after a transient period much shorter than T_2, unless the refocusing pulses are perfect 180° (Fig. 1b). This behavior is well-known, and corresponds to the refocusing sequences CPMG and CP, respectively [25]. In the general case, the phase of the magnetization is given by Eq. (1) and is neither 0° nor 90°, thus the behavior of the magnetization during the refocusing train is not trivial (Fig. 1c). However, by considering the initial magnetization as the sum of two orthogonal components, parallel and perpendicular to the refocusing pulses, the evolution can be understood based on the CPMG and CP behaviors. From this point on, we will denote these two components as CPMG- and CP-components.

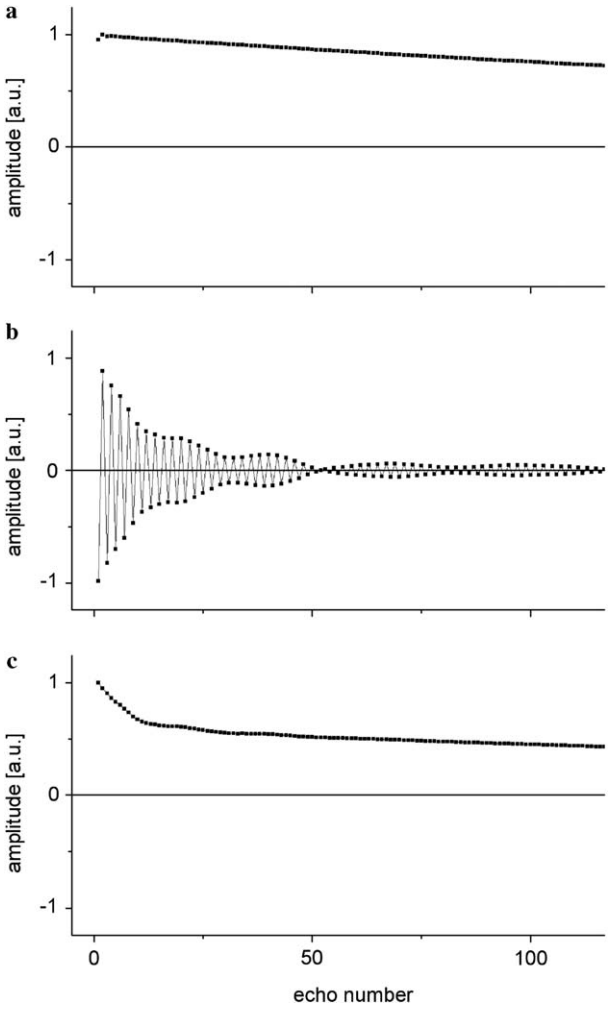

Fig. 1. (a) Echo amplitude decay for the CPMG sequence. The excitation pulse is applied with phase $\phi = 0°$, and the refocusing pulses with phase 90°. (b) Echo amplitude decay for the CP sequence $\phi = 90°$. (c) The excitation pulse has phase $\phi = 60°$. The experiments were obtained using a 10 mm birdcage rf coil. A 10 mm diameter tube containing pure water (10 mm height) was placed in the center of the rf coil. The best 180° pulse was calibrated by maximizing the lifetime of the signal in the CP experiment.

2.3. The problem

The average propagator $P(\mathbf{R})$ is a real (and positive valued) function. Thus the $\mathbf{q}$-space signal $S(\mathbf{q})$, which is the Fourier transform of the propagator, obeys complex conjugate symmetry, i.e. $S(\mathbf{q}) = S^*(-\mathbf{q})$. In general, $S(\mathbf{q})$ can be written as a complex function consisting of an even real part and an odd imaginary part:

$$S(\mathbf{q}) = S(\mathbf{q})_{\mathrm{Re}} + \mathrm{i}S(\mathbf{q})_{\mathrm{Im}} \tag{4}$$

for which

$$S(-\mathbf{q})_{\mathrm{Re}} = S(\mathbf{q})_{\mathrm{Re}} \quad \text{and} \tag{5}$$

$$S(-\mathbf{q})_{\mathrm{Im}} = -S(\mathbf{q})_{\mathrm{Im}}. \tag{6}$$

As is well-known from the properties of Fourier transforms (FT), the FT of a real and even function is also a real and even function, whereas the Fourier transform of an imaginary, odd function is a real and odd function:

$$\mathrm{FT}\{S(\mathbf{q})_{\mathrm{Re}}\} = P(\mathbf{R})_{\mathrm{Re,\ even}} \tag{7}$$

$$\mathrm{FT}\{\mathrm{i}S(\mathbf{q})_{\mathrm{Im}}\} = P(\mathbf{R})_{\mathrm{Re,\ odd}} \tag{8}$$

The average propagator measured is a sum of even and odd contributions arising from the Fourier transforms of the real and imaginary components of $S(\mathbf{q})$.

$$P(\mathbf{R})_{\mathrm{meas}} = P(\mathbf{R})_{\mathrm{Re,\ even}} + P(\mathbf{R})_{\mathrm{Re,\ odd}} \tag{9}$$

Naturally, if the amplitudes of either the real and imaginary $\mathbf{q}$-space signal are weighted by some arbitrary constants c_{Re} and c_{Im}, this will lead to false $\mathrm{P}(\mathbf{R})$ if $c_{\mathrm{Re}} \neq c_{\mathrm{Im}}$:

$$\begin{aligned} P(\mathbf{R})_{\mathrm{meas}} &= \mathrm{FT}\{c_{\mathrm{Re}}S(\mathbf{q})_{\mathrm{Re}}\} + \mathrm{FT}\{c_{\mathrm{Im}}S(\mathbf{q})_{\mathrm{Im}}\} \\ &= c_{\mathrm{Re}}P(\mathbf{R})_{\mathrm{Re,\ even}} + c_{\mathrm{Im}}P(\mathbf{R})_{\mathrm{Re,\ odd}} \end{aligned} \tag{10}$$

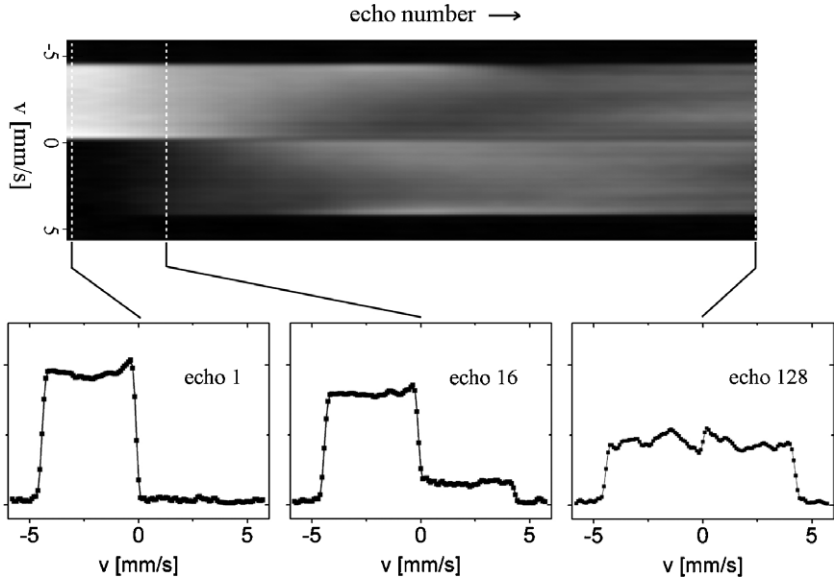

Fig. 2. Top, propagators of water flowing through a cylindrical tube as a function of the echo number measured with the SE+CPMG sequence using a 20 mm birdcage rf coil. Due to oscillating behavior of the CP-component the sign of the velocity axis was inverted for propagators obtained from even echoes. The propagators from echoes 1, 16, and 128 are shown on the bottom. Although the propagator obtained from the first echo is perfectly encoded, the phase information is progressively lost from echo to echo, leading to mirrored propagators for large echo numbers.

In a multiecho PFG NMR experiment, these "constants" can depend on the signal decay, i.e. $c_{\mathrm{Re}} = c_{\mathrm{Re}}(nT_{\mathrm{E}})$ and $c_{\mathrm{Im}} = c_{\mathrm{Im}}(nT_{\mathrm{E}})$, where $n = 1, 2, 3, \ldots$ is the number of the echo, and T_{E} is the echo time. Under real experimental conditions, the sign of the velocity in the resulting function $P(\mathbf{R})$ is eventually lost as one of its even or odd components approaches zero.

In order to show this effect, the rectangular propagator of Poiseuille flow through a cylindrical tube was taken as an example. It can be decomposed, according to Eq. (10), into a sum of the even and odd contributions stemming from the real and the imaginary part of the signal $S(\mathbf{q})$, respectively. A Fourier transformation of the first echo with respect to $\mathbf{q}$ reproduces the almost undistorted propagator (Fig. 2), showing that for this echo $c_{\mathrm{Re}} = c_{\mathrm{Im}}$. However, due to pulse imperfections, the CP-component approaches zero as the echo number increases. As a consequence, even and odd components become unbalanced, and the propagator for large echo numbers represents the velocity range while information about the velocity sign becomes lost.

2.4. Solutions

Several multiecho sequences have been suggested to preserve the phase of the transverse magnetization during the refocusing train. They reduce cumulative effects due to imperfect refocusing pulses by cycling their phase during the train. Two main families can be distinguished, called MLEV [26] and XY [27,28]. Depending on the phase cycling loop length, for instance 8, the sequences assume the names MLEV-8 and XY-8, respectively. The advantage of high order (n) of the refocusing loops is the improved tolerance to imperfect pulses. The drawback is that only the phases of every (n/2)th echo are coherent.

To clarify this concept the evolution of the magnetization phase for a XY-4 and MLEV-4 are shown in Fig. 3. The magnetization vectors correspond to the time of the echo formation. For the case of XY-4, only one in four echoes has strictly the same phase, however by changing the receiver phase by 180°, every other echo can be used. At first sight, one might conclude that it is also possible to use all echoes if corrections such as $(M_x, M_y) \rightarrow (-M_x, M_y)$ are made. However, this transformation can only be applied at the echo maximum; an instant of time before or after the echo formation the magnetization is mixed, M_x does not correspond any longer to its correct value (M_x^i in Fig. 3). Furthermore, if phase encoding is used like in the PEPI or RARE sequences, even at the echo maximum the two components of the magnetization are mixed.

Fig. 4a shows the evolution of one component of the magnetization as a function of the echo number for the MLEV-4 sequence. Every other echo is displayed. The ratio T_2/T_{E} was chosen to 256, thus 128 echoes can be effectively used until the signal amplitude decreases to $1/e$ of its initial value (flip angle 180°). Although for the case of 180° the decay is monoexponential as expected, when the flip angle deviates from the ideal value the echo amplitude decays faster and does even oscillate from positive to negative values. In the case of the RARE sequence, the phase encoding direction will be strongly distorted even for small deviations from the ideal 180° condition. Fig. 4b shows the point spread function (PSF) [29] along the phase encoding direction for a flip angle of 140°. In order to avoid such a PSF the following criterion can be taken: the maximum number of echoes available for a given case

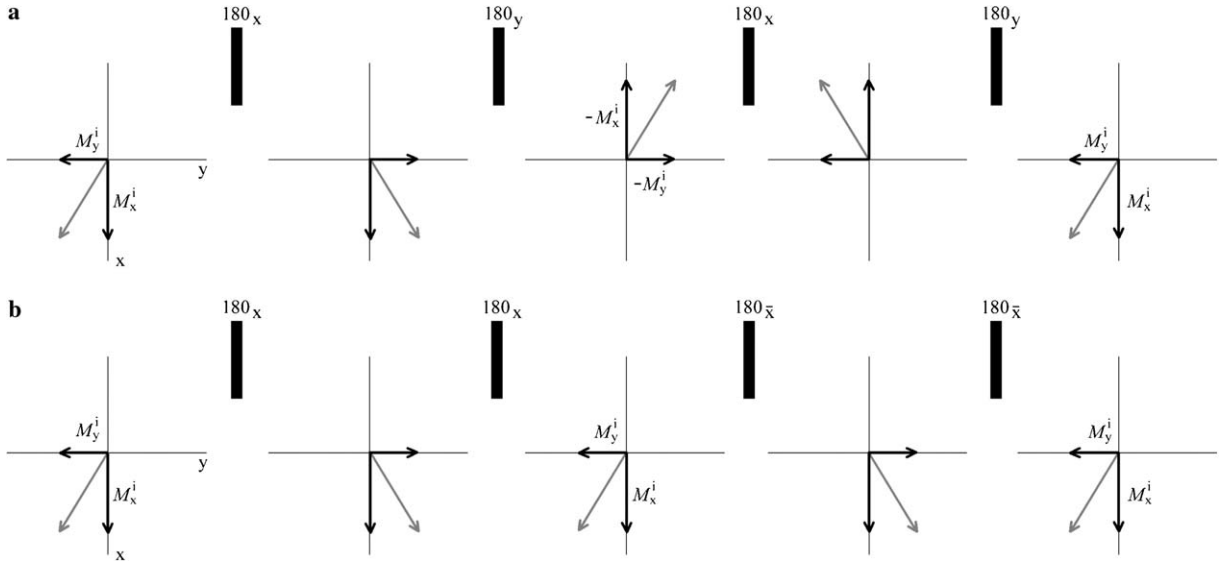

Fig. 3. (a) Evolution of the magnetization for the XY-4 sequence. The magnetization vectors correspond to the time of the echo formation, thus phases due to static field inhomogeneities and chemical shift are refocused. Perfect 180° pulses and absence of relaxation were assumed. Although the initial magnetization phase is recovered only after multiples of four pulses, by changing the receiver phase by 180° this holds for every other echo. (b) The same as (a) but for the MLEV-4 sequence.

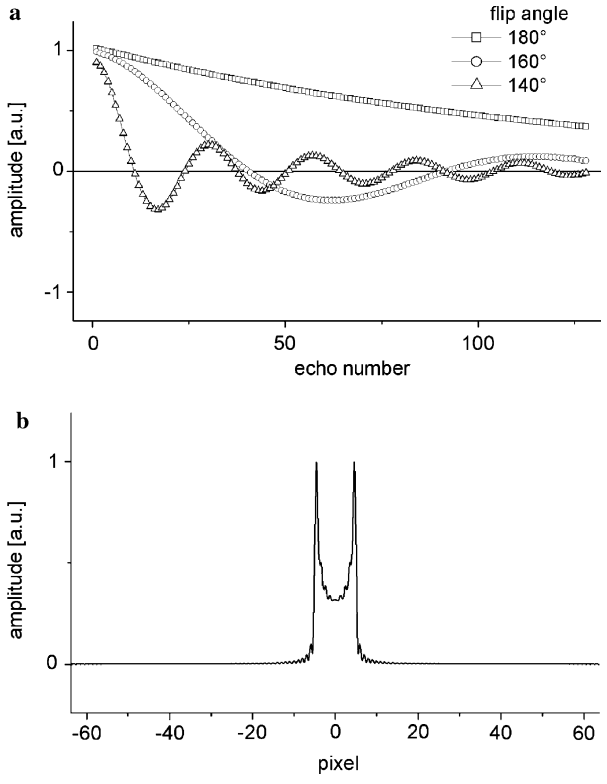

Fig. 4. (a) Amplitude of one component of the echo as a function of the echo number for the MLEV-4 sequence. Although only one component is shown, the second one has the same behavior. For the calculations the following parameters were considered: $T_1 = 3$ s, $T_2 = 1$ s, $T_E = 3.9$ ms, homogenous B_1, and a resonance frequency distribution that assures a spreading of the transverse magnetization before the 180° pulses are applied ($T_2^* < T_E/2$). For a perfect refocusing pulse (180°) the decay is exponential as expected, however as the flip angle is reduced, the magnetization oscillates and approaches zero in a time shorter than T_2. (b) FT of the amplitude envelope for flip angles of 140°. In the case of a RARE sequence it is the PSF along the phase encoding.

is defined as the decay of the signal intensity to $1/e$ of its initial amplitude.

We used this criterion to evaluate the performance of several sequences as a function of the flip angle. The results are summarized in Fig. 5. In the case of the CPMG scheme, since both components must by considered, the limit is fully determined by the decay of the CP-component. Due to the oscillation of the CP-component (Fig. 1b) every other echo was considered. It is remarkable that even for an error of 0.5° the maximum number of echoes drops down by a factor of one-half. In contrast, MLEV-4 has an almost flat response in the range of ±5°. However, after this limit the performance also degrades very fast reaching 64 echoes for an error of ±12°. For higher order MLEV loops, the response is flat in a much larger range of flip angles, for example ±30° for the MLEV-16, however the limitation

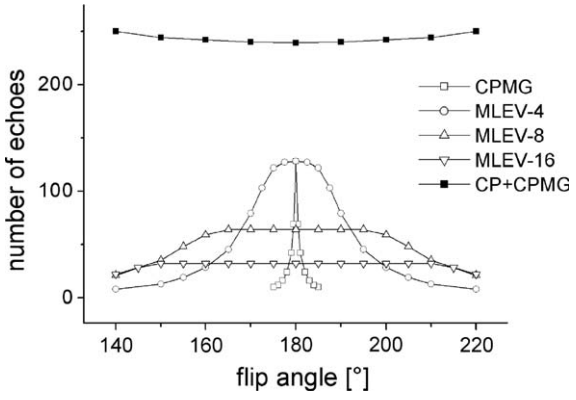

Fig. 5. Performance of several sequences as a function of the flip angle. The maximum number of echoes, which can be used, is defined as the decay to $1/e$ of the initial amplitude (see text). Parameters are as in Fig. 4.

of acquiring only every (n/2)th echo is determinant. The performance of the XY-4, -8, and -16, not shown in the plot, were also studied obtaining a similar behavior as for their respective MLEV loops. We also analyzed the case of composite refocusing pulses [17], but this performance was slightly inferior to that of the order 4 loops.

In contrast to the above methods, which are intended to preserve both magnetization components during the train, we have recently presented an approach that preserves only one component per experiment. Thus, two experiments switching the phase of the refocusing pulses by 90° are used to sample the CP- and CPMG-components one by one [30–33]. A similar method, making use of soft- and slice-selective rf pulses, has been presented in a very recent contribution to this journal [34]. The robustness of the approach can be judged from Fig. 5. It is worth noting that both even and odd echoes can be used, improving already the performance for the case of perfect 180° pulses by a factor 2. Furthermore, in the cases of a flip angle $180° \pm 40°$ the performance of the CP+CPMG method is by more than one order of magnitude better than the best performing MLEV loop. The slightly increasing number of echoes available when moving away from the 180° condition is a consequence of a small admixture of T_1 to T_2, resulting in a longer $T_{2\text{eff}}$, an effect commonly observed in pulse trains with pulses deviating considerably from the 180° optimum. Besides a short transient period during the first echoes, the sequence can be used even with flip angles as low as 90°. In this case, 90°, after eliminating the first 16 echoes, the echo train decays exponentially.

3. Velocity-imaging sequence

A RARE like imaging sequence, preceded by a velocity-encoding module, is displayed in Fig. 6. The velocity-encoding period is a conventional PGSE, combined with a slice selective excitation rf pulse. The signal output of this period is an echo that is phase-encoded by displacement. Following it, a "filter" is applied in order to preserve the magnetization component in phase with the refocusing train while spoiling the perpendicular one. For example, if the refocusing pulses are applied with phase y, only the CPMG-component is preserved while the CP-component oscillates and decays as shown in Fig. 1b. Because of the imaging gradients the two components are mixed during the train, thus it is not possible to eliminate one of them simply by data processing. Hence, the filter is a critical component that must be applied preceding the multiecho imaging loop. The final sequence requires a total of four signal acquisition shots with appropriate pulse phases for generating a full velocity-encoded image. Due to the independent phase encoding of each echo in the imaging period the trajectory in **k**-space can be freely chosen to enhance contrast by relaxation, like it is done in a conventional RARE sequence [9]. It must be stressed that a method like PEPI, based on an accumulative phase encoding from echo to echo, cannot be implemented with the proposed

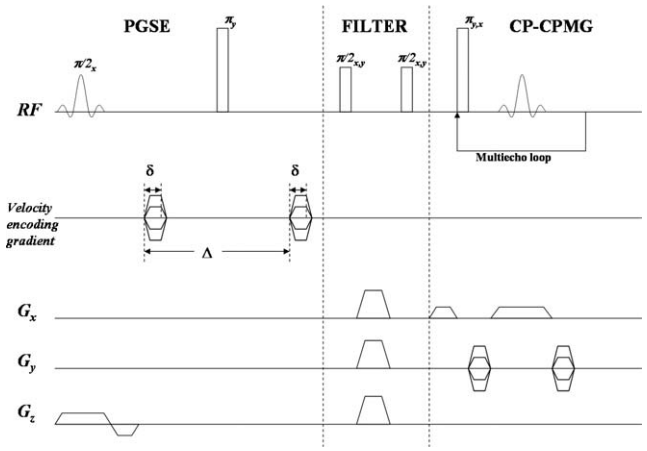

Fig. 6. Velocity-imaging sequence. The sequence is divided into three periods: velocity encoding, filtering, multiecho imaging. The phase of the refusing pulses is cycled between x and y to sample the CP- and CPMG-components independently. Notice that the phases of the filter must also be cycled.

CP+CPMG phase cycling because it preserves one component and not the full magnetization during the echo train.

Regarding the velocity encoding period, although a spin echo method was chosen, it can be replaced by a stimulated-echo-based sequence without the need of further modifications on the filtering and imaging periods. Moreover, the extension to 3D imaging by introducing a second phase encoding gradient is straightforward. However, it must be emphasized that any extra encoding which modifies the phase of the signal has to be applied prior the filtering period.

4. Experiments and results

All experiments were performed on a Bruker DMX 300 MHz spectrometer equipped with a horizontal bore 7 T magnet employing a Bruker MICRO2.5 gradient system. Experiments were carried out either with a Bruker birdcage microimaging resonator of 20 mm diameter, or with a single-turn circular surface coil 15 mm diameter which was wound from copper wire 1.5 mm thick.

To illustrate the performance of the method, first, the rectangular propagator of Poiseuille flow through a cylindrical tube was measured. For this experiment, the imaging phase and read gradients of the sequence of Fig. 6 were set to zero. A series of propagators obtained independently from each echo is shown in Fig. 7. This experiment is in agreement with calculated results of Fig. 5, and experimentally proves the robustness of the CPMG+CP approach.

As a second experiment, the same geometry was studied, with a surface rf coil and in combination with imaging. The method was used first to measure propagators at three different depths with respect to the rf coil. Then, inside each slice, the propagator was spatially resolved to measure the velocity pixel by pixel, obtaining the 1D velocity maps of Fig. 8. All profiles show the expected dependence of the

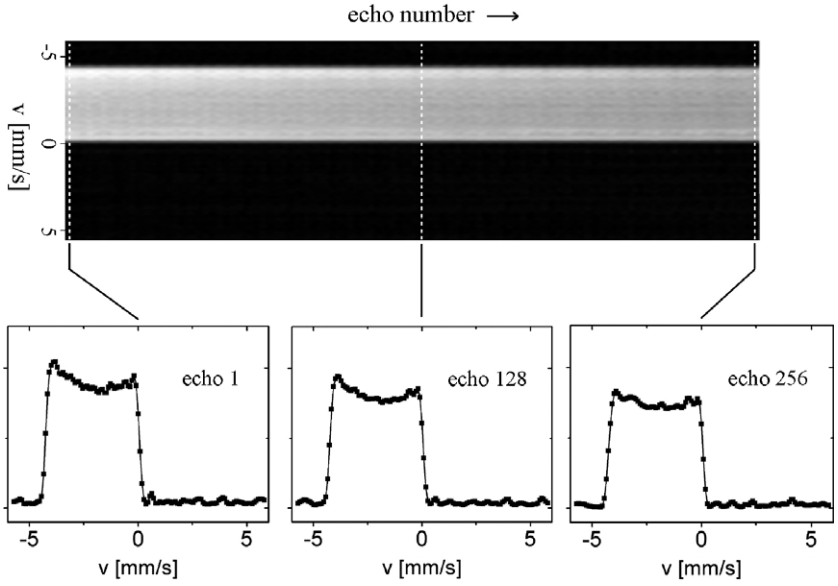

Fig. 7. The same as Fig. 2, yet implementing the CPMG+CP approach. The experiment was obtained by using the sequence of Fig. 6 without imaging gradients. The following experimental parameters were used: $\Delta = 90$ ms, $\delta = 1$ ms, maximum gradient 0.18 T/m, 32 steps to sample the **q**-space from negative to positive values. To avoid outflow a 5 mm thick slice was selected perpendicular to the flow direction.

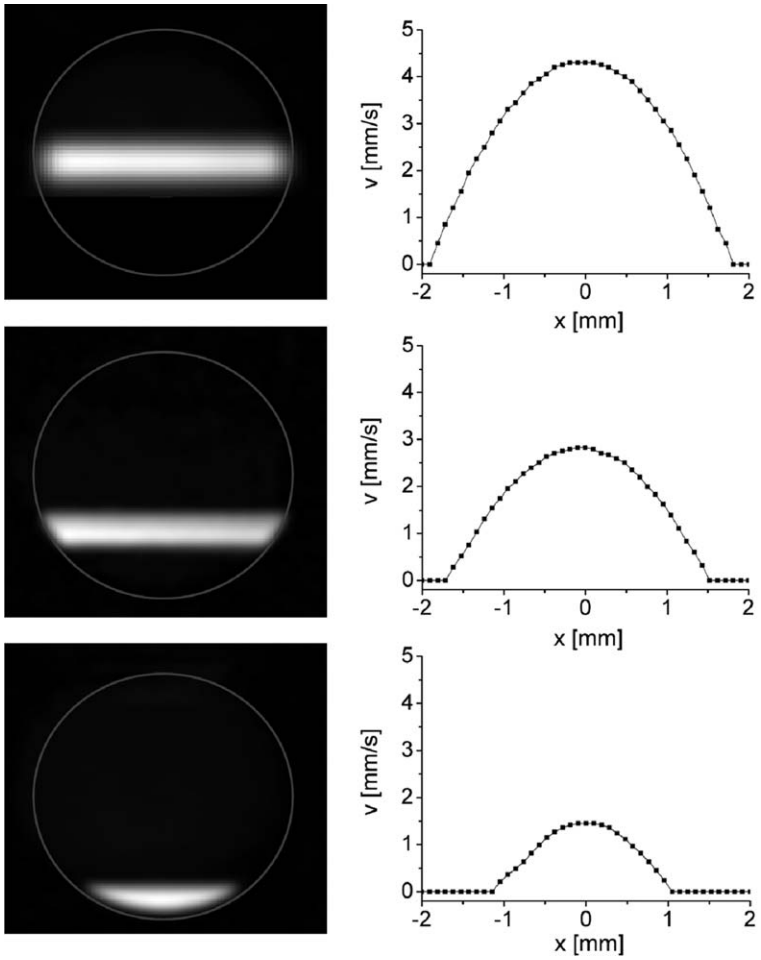

Fig. 8. The left column shows 2D images obtained from three selected slices at three different positions with respect to the surface coil. The right column shows the respective velocity maps (1D) calculated from propagator measurements. The experiment was obtained by implementing the sequence of Fig. 6, replacing the hard 180° pulse of the PGSE by a soft one. This pulse was used to select the slices shown in the figure. The experimental parameters related to the PGSE are the same as in Fig. 7. The images have 64×64 pixels and a FOV of 4.5×4.5 mm^2.

velocity on position as well as the decrease of the maximum velocity when approaching the pipe wall. Both are a consequence of the parabolic velocity distribution with respect to the radial coordinate; due to the velocity distribution within the finite slice thickness in the bottom image of Fig. 8, the corresponding profile is not parabolic itself.

The method was finally implemented to measure the local velocity in two pipes with water flowing in opposite directions. Besides proving the validity of the method with another example, this experiment has the aim of showing typical distortions, and how they might lead to wrong interpretations in situations of more complicated flow patterns. The spatial resolution was set fine enough to assure, to a good approximation, a single velocity value per pixel. In this limit, the velocity can be measured either by sampling the full **q**-space or by using a single step in the velocity encoding gradients. The velocity is then measured from the propagator or by calculating a phase difference between two experiments, respectively. Fig. 9a shows the velocity map obtained by implementing the sequence of Fig. 6. The two axially symmetric paraboloids with opposite sign are in good agreement with the expected Hagen–Poiseuille flow conditions. Although the displayed results correspond to the full propagator approach, the single-step method showed the same behavior but with the expected lower signal-to-noise ratio. In Fig. 9b, only the CPMG-component of the signal is used. Due to the loss of the CP-component the propagators become mirrored as shown in Fig. 2. Therefore, when searching for the maximum amplitude in the propagator, values corresponding to positive and negative velocities are equally probable. Because of noise, the algorithm finds sometimes positive, sometimes negative values, leading to the pattern of Fig. 9b. If the condition $v > 0$ is introduced, the jumping from positive to negative values is eliminated, and two axially symmetric paraboloids are obtained once more (Fig. 9c). Thus, one might conclude that the method is working, with the exception of a sign ambiguity that might become more serious if both positive and negative velocities exist, for instance in flow through a structured medium. The last two results were obtained from the full propagator measurement. Instead, one can use the single-step approach, obtaining the result of Fig. 9d. In this case, the loss of the CP-component is critical. With only one component it is not possible to calculate the phase introduced by the velocity; it is undetermined and fluctuates about zero. Consequently, the phase difference also remains approximately zero, and no velocity information can be extracted from the image.

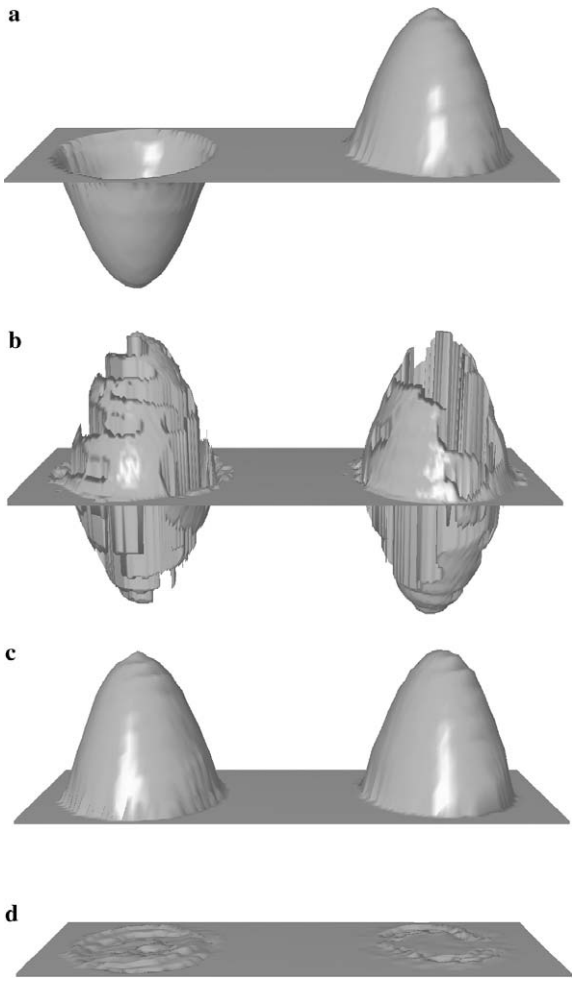

Fig. 9. (a) Velocity map of two pipes with water flowing in opposite directions obtained with a surface coil using the sequence of Fig. 6. (b) Same as (a) but with only the CPMG component. The jumps in the velocity are due to mirroring of the propagator. This is overcome by introducing the condition $v > 0$ (c). (d) Same as (b) yet using the two step approach to measure the velocity by calculating the phase shift pixel by pixel.

5. Conclusions

Velocity measurements with spatial resolution, in particular multi-dimensional velocity imaging, are of growing interest to engineering and biomedical applications, but their combination with fast-imaging schemes faces a number of restrictions. Most important of these is the need for preserving the sine and cosine components of the signal in order to reconstruct the correct velocity information. This can be achieved under ideal situations, but even a relatively small inhomogeneity of the B_1 field results in a position-dependent deviation of the pulse flip angle from the ideal 180° that is sufficient to generate a cumulative effect for a long pulse train; multiecho sequences are thus always compromised by the efficiency of rf pulses to maintain the correct signal phase throughout the sequence. In this paper, we have validated, based on numerical simulations, the number of "useful" echoes for velocity imaging for several commonly used phase cycling schemes, and have suggested a combination of CPMG and CP schemes with appropriate filter pulses between the velocity encoding and multiecho-imaging modules. This scheme is robust and provides optimum results even in conditions of severe B_1 inhomogeneities. Despite requiring four acquisition runs with appropriate pulse phases, it is still considerably faster than

single-echo methods as it allows the acquisition of one velocity encoding component of a 2D image within one single echo train. It furthermore avoids the necessity of using composite pulses which introduce some limitations with respect to hardware, bandwidth and T_2^* of the sample under study. The method is easy to implement and suitable for obtaining spatially resolved velocity information particularly in environments where a compromise between rf coil homogeneity and signal intensity must be made, potentially allowing the investigation of transient flow processes with good temporal resolution.

Acknowledgments

S.A. thanks the Academy of Finland and the Finnish national graduate school of computational chemistry and molecular spectroscopy (LASKEMO) for funding.

References

[1] E.A. Zerhouni, D.M. Parrish, W.J. Rodgers, A. Yang, E.P. Shapiro, Human-Heart-tagging with MR imaging—a method for non-invasive assessment of myocardial motion, Radiology 169 (1988) 59–63.
[2] M.V. Icenogle, A. Caprihan, E. Fukushima, Mapping flow streamlines by multistripe tagging, J. Magn. Reson. 100 (1992) 376–381.
[3] L.G. Raguin, J.G. Georgiadis, Kinematics of the stationary helical vortex mode in Taylor–Couette–Poiseuille flow, J. Fluid Mech. 516 (2004) 125–154.
[4] J.C. Gatenby, J.C. Gore, Echo-planar-imaging studies of turbulent flow, J. Magn. Reson. A121 (1996) 193–200.
[5] B. Manz, P.S. Chow, L.F. Gladden, Echo-planar imaging of porous media with spatial resolution of 100 μm, J. Magn. Reson. 136 (1999) 226–230.
[6] A.J. Sederman, M.D. Mantle, L.F. Gladden, Single excitation multiple image RARE (SEMI-RARE): ultra-fast imaging of static and flowing systems, J. Magn. Reson. 161 (2003) 15–24.
[7] A. Haase, J. Frahm, D. Matthei, W. Hänicke, K.D. Merboldt, FLASH imaging: rapid NMR imaging using low flip angles, J. Magn. Reson. 67 (1986) 258–266.
[8] P. Mansfield, P.G. Morris, NMR imaging in biomedicine, Adv. Magn. Res. 1–343 (Suppl. 2) (1982).
[9] J. Hennig, A. Nauerth, H. Freidburg, RARE imaging: a fast imaging method for clinical MR, Magn. Reson. Med. 3 (1986) 823–833.
[10] B. Newling, C.C. Poirier, Y. Zih, J.A. Rioux, A.J. Coristine, D. Roach, B.J. Balcom, Velocity imaging of highly turbulent gas flow, Phys. Rev. Lett. 93 (2004) 154503.
[11] R.W. Mair, C.H. Tseng, G.P. Wong, D.G. Cory, R.L. Walsworth, Magnetic resonance imaging of convection in laser polarized Xenon, Phys. Rev. E61 (2000) 2741.
[12] M. Rokitta, U. Zimmermann, A. Haase, Fast NMR flow measurements in plants using FLASH imaging, J. Magn. Reson. 137 (1999) 29–32.
[13] K. Kose, Instantaneous flow-distribution measurement of the equilibrium turbulent region in a circular pipe using ultrafast NMR imaging, Phys. Rev. A 44 (1991) 2495–2504.
[14] K. Kose, One-shot velocity mapping using multiple spin-echo EPI and its application to turbulent flow, J. Magn. Reson. 92 (1991) 631–635.
[15] K. Kose, Visualization of local shearing motion in turbulent fluids using echo-planar imaging, J. Magn. Reson. 96 (1992) 596–603.
[16] A.J. Sederman, M.D. Mantle, C. Buckley, L.F. Gladden, MRI technique for measurement of velocity vectors, acceleration, and autocorrelation functions in turbulent flow, J. Magn. Reson. 166 (2004) 182–189.
[17] S. Han, P.T. Callaghan, One-shot velocimetry using echo planar imaging microscopy, J. Magn. Reson. 148 (2001) 349–354.
[18] D.N. Guilfoyle, P. Mansfield, K.J. Packer, Fluid-flow measurement in porous-media by echo-planar imaging, J. Magn. Reson. 97 (1992) 342–358.
[19] T.W.J. Scheenen, D. van Dusschoten, P.A. de Jager, H. Van As, Microscopic displacement imaging with pulsed field gradient turbo spin-echo NMR, J. Magn. Reson. 142 (2000) 207–215.
[20] B. Manz, Combined relaxation and displacement experiment: a fast method to acquire T_2, diffusion and velocity maps, J. Magn. Reson. 169 (2004) 60–67.
[21] P.T. Callaghan, Principles of Nuclear Magnetic Resonance Microscopy, Oxford University Press, Oxford, 1991, p. 438.
[22] B. Manz, P.T. Callaghan, Velocity exchange spectroscopy, J. Magn. Reson. A 106 (1994) 260–265.
[23] S. Ahola, F. Casanova, J. Perlo, K. Münnemann, B. Blümich, S. Stapf, Monitoring of fluid motion in a micromixer by dynamic NMR microscopy, Lab on a Chip 6 (2006) 90–95.
[24] J. Kärger, W. Heink, The propagator representation of molecular-transport in microporous crystallites, J. Magn. Reson. 51 (1983) 1–7.
[25] S. Meiboom, D. Gill, Modified spin-echo method for measuring relaxation times, Rev. Sci. Instrum. 29 (1958) 688–691.
[26] M.H. Levitt, R. Freeman, T. Frenkiel, in: J.S. Waugh (Ed.), Advances in Magnetic Resonance, Academic Press, New York, 1983.
[27] A.A. Maudsley, Modified Carr–Purcell–Meiboom–Gill sequence for NMR fourier imaging applications, J. Magn. Reson. 69 (1986) 488–491.
[28] T. Gullion, D.B. Baker, M.S. Conradi, New, compensated Carr–Purcell sequences, J. Magn. Reson. 89 (1990) 479–484.
[29] A.G. Webb, Optimizing the point spread function in phase-encoded magnetic resonance microscopy, Concept Magn. Reson. 22A (2004) 25–36.
[30] F. Casanova, J. Perlo, B. Blümich, K. Kremer, Multi-echo imaging in highly inhomogeneous magnetic fields, J. Magn. Reson. 166 (2004) 76–81.
[31] J. Perlo, F. Casanova, B. Blümich, 3D imaging with a single-sided sensor: an open tomograph, J. Magn. Reson. 166 (2004) 228–235.
[32] F. Casanova, J. Perlo, B. Blümich, Velocity distributions remotely measured with a single-sided NMR sensor, J. Magn. Reson. 171 (2004) 124–130.
[33] J. Perlo, F. Casanova, B. Blümich, Velocity imaging by ex-situ NMR, J. Magn. Reson. 173 (2005) 254–258.
[34] P. Galvosas, P.T. Callaghan, Fast magnetic resonance imaging and velocimetry for liquids under high flow rates, J. Magn. Reson. 181 (2006) 118–124.